Applied Physics A (2021) 127:509
https://doi.org/10.1007/s00339-021-04668-6

Applied Physics A
Materials Science & Processing

Graphene-coated micro/nanostructure hard carbon with improved electrochemical performance for sodium-ion battery

Guo Jialin[1] · Peng Zheng[2]

Received: 9 March 2021 / Accepted: 3 June 2021 / Published online: 10 June 2021

Abstract
Surface area and conductivity are important indexes for the hard carbon as the anode for a sodium-ion battery. Through a different treatment, pine needle derived bulk and micro/nanostructured hard carbons were obtained, respectively. Due to some Na-ions could be stored in the nanopores, the small surface area of the bulk amorphous carbon (1.2 $m^2 g^{-1}$) resulted in a low capacity than that of micro/nanostructure carbon (141 $m^2 g^{-1}$). In order to further improve the performance, rGO coating is employed for the micro/nanostructure carbon by a one-step high temperature annealing process. Due to the enhanced electrical conductivity, the composite displays the capacity of 281 mAh g^{-1} at 20 mA g^{-1}, which is improved by 68%. Well rate performance and long-cycle stability are also obtained. Considering the improved performance and bio-renewable advantage, the micro/nanostructure hard carbon derived from pine needle coated with rGO would be a suitable anode material for SIBs.

Keywords Pine needle · Hard carbon/rGO composite · Anode material · Sodium-ion battery

1 Introduction

Due to the moderate energy density and long-term cycling, lithium-ion batteries (LIBs) have been used widely as power source for portable electronics [1–3]. The terrestrial reserve of lithium hinders their application in large-scale energy storage for electric vehicles (EVs) and hybrid electric vehicles (HEVs), as well as for stationary energy storage for wind and solar energy [4]. As a promising alternative to LIBs, sodium-ion batteries (SIBs) attract much attention because of their low cost, similar physical chemistry property and widespread availability of sodium resources [5–7].

Although the working mechanism of SIBs is similar to that of LIBs, the larger ionic radius of Na-ion (1.02 Å) than that of the Li-ion (0.76 Å) makes most anodes for LIBs invalid as the electrode for SIBs [8–10]. Graphite is the typical case of this, which has the theoretical capacity of 372 mAh g^{-1} for LIBs, but only exhibits 31 mAh g^{-1} for SIBs [11–13]. TiO_2 [14], MXene [15], and MoS_2 [16] show high capacities as the anodes of SIBs, but the large expanded volume and bad cycle stablities are the barrier of these electrode materials. For electrolyte, photopolymer electrolytes [17], MOF derived solid-state electrolytes [18], and ultralow-concentration electrolyte [19] are the newly appeared topics in the electrolyte of SIBs. Carbon-based materials still have been given much attention as the anode of SIBs, because of the merits of structure stability, low cost and renewable of carbon. Among various kinds of carbon, hard carbon is regarded as the promising candidate with its house card mode and nanoporous structure which could accommodate more Na ions [20–22]. Generally, it is hard carbon for most biomass derived carbon. Due to the abundance, low cost and easy accessibility, biomass derived carbons have been extensively investigated as the anode of SIBs, for example sucrose [23], walnut shell membranes [24], pomelo peels [25] and paper [26] had shown satisfying performance. The electronic conductivity of hard carbon is lower than that of graphite, which would limit the capacity and rate performance of anodes [27].

Due to the high electronic conductivity and well structure flexibility of graphene, we employ it as the electric conduction frame to couple biomass derived hard carbon.

✉ Guo Jialin
Jialin_G@163.com

[1] Shaanxi Key Laboratory of Comprehensive Utilization of Tailings Resources, College of Chemical Engineering and Modern Materials, Shang Luo University, 726000, Shang Luo, Shaanxi, People's Republic of China

[2] School of Materials Science and Engineering, Shaanxi University of Science and Technology, Xian 710021, Shaanxi, People's Republic of China

For biomass precursor, as the diversity structure of the biomass precursors, to further enrich the exploration biomass kind for SIBs, we choose pine needle as biomass precursor owing to its tremendous yields and widespread distribution. In this paper, through hydrothermal and high temperature annealing process of pine needle, micro/nanostructure hard carbon (named as HTPC) was obtained. It shows high first-cycle columbic efficiency. To further enhance its capacity, the derived hard carbon/reduced graphene oxide composite (denoted as HTPC/rGO) was fabricated through a simple annealing process. The composite exhibits well rate performance (156 mAh g^{-1} at 200 mA g^{-1}) and high capacity of 281 mAh g^{-1} (improved 68% compared with the bare HTPC).

2 Experimental

To make sure of the reproducibility, the raw material of pine needle was collected from three cities of Xi'an, Shangluo, and Taiyuan, respectively. It was washed by deionized water and alcohol, then dried at 60 °C for 12 h. For the synthesis of bulk carbon, 5 g of pine needle precursor was loaded in a tubular furnace and heated at 800 °C for 2 h (ramp rate: 5 °C min^{-1}) under argon atmosphere. The obtained product was ground and washed with 1 M HCl and deionized water again. After drying at 80 °C for 12 h, the product was termed as DPC. For the synthesis of micro/nanostructure carbon, 3 g of pine needle precursor and 35 mL deionized water were placed in a 50 mL Teflon-lined autoclave and heated at 160 °C for 10 h. After being cooled to room temperature naturally, the solid product was collected and washed with 1 M HCl and deionized water. The obtained solid product was further annealed at 800 °C (heating rate, 5 °C min^{-1}) for 2 h under Ar atmosphere, and the final product was labeled as HTPC. Graphene oxide was synthesized from graphite flakes according to the modified Hummers methods, as reported elsewhere [28]. To prepare HTPC/rGO composite, a homogeneous GO suspension was obtained by sonicating GO (10 mg) in absolute ethanol (100 mL) for 30 min. The suspension obtained was then mixed with HTPC (100 mg) under violent stirring to form the HTPC/GO hybrid. After centrifuged and dried, the sample was annealed at 800° C for 1 h under Ar atmosphere to generate HTPC/rGO composite.

X-ray powder diffraction (XRD) patterns were acquired on a Rigaku D/MAX2200PC diffractometer operated at room temperature with Cu Kα ($\lambda = 1.54178$ Å) radiation. Raman spectra were recorded at room temperature on a Renishaw-invia confocal Raman microscope system equipped with a 532 nm laser excitation. The morphologies of as-prepared carbon materials were observed by scanning electron microscopy (SEM) (Rigaku S4800) and transmission electron microscopy (TEM, JEM 2100). The nitrogen adsorption/desorption analysis was done at 77 K on a Micromeritics ASAP 2020 apparatus.

The electrochemical property measurements were conducted on 2032 coin cells. The working electrode was prepared by mixing the as-obtained carbon materials, conducting agent (Super P) and polyvinylidene fluoride (PVDF) (in N-methyl-2-pyrrolidone) with a weight ratio of 80: 10: 10. The obtained slurry was coated onto a copper foil and dried at 120 °C for 10 h under vacuum. The foil was finally cut into circle disks with diameter of 16 mm, which were used as the anode in the 2032 coin cells. Besides, the pure Na foil was utilized as a counter electrode and reference electrodes, glass fibers (GF/D) from Whatman were used as separator, and 1.0 mol L^{-1} $NaClO_4$ in ethylene carbonate/propylene carbonate (1:1 v/v) was used as electrolyte. All the coin cells were assembled in argon-filled glove box. The charge–discharge tests were performed on a Newaresles battery test system (BTS) (Shenzhen, China) in a voltage range of 0.01–3.0 V at different current rates. The capacity was calculated based on the mass of active material. Cyclic voltammetry (CV) was carried out at room temperature on an electrochemical workstation (CHI 660E).

3 Results and discussion

The pine needle is a lignocellulosic material [29]. To guarantee the reproducibility of the product, pine needle used in this article is selected from three cities of Xi'an, Shangluo, and Taiyuan, respectively. As confirmed by the elemental analysis testing (Table 1), the contents of C and O in pine needle from these three regions had no large difference. The morphologies of the pristine pine needle from these three regions were the same, as shown as scanning electron microscopy (SEM); they are composed of particles with the size smaller than 1 μm, and the particles are contacted closely with each other (Fig. 1a). If pyrolysis it directly at 800 °C under Ar atmosphere, the product (denoted as DPC) is bulk with smooth surface (Fig. 1b). As they had reported [30], the pre-hydrothermal treatment can relieve the crosslinking and produce small particles, so we employ it before high temperature pyrolysis. Figure 1c displays the morphology of chars derived from pine needle after hydrothermal treatment; they are nanoparticles and spheres with the size of 1 μm. When further pyrolysis process happened

Table 1 C and O contents of the pine needle form the three regions estimated by elemental analysis

	Xi'an (%)	Shangluo (%)	Taiyuan (%)
C	52	55	53
O	42	41	43

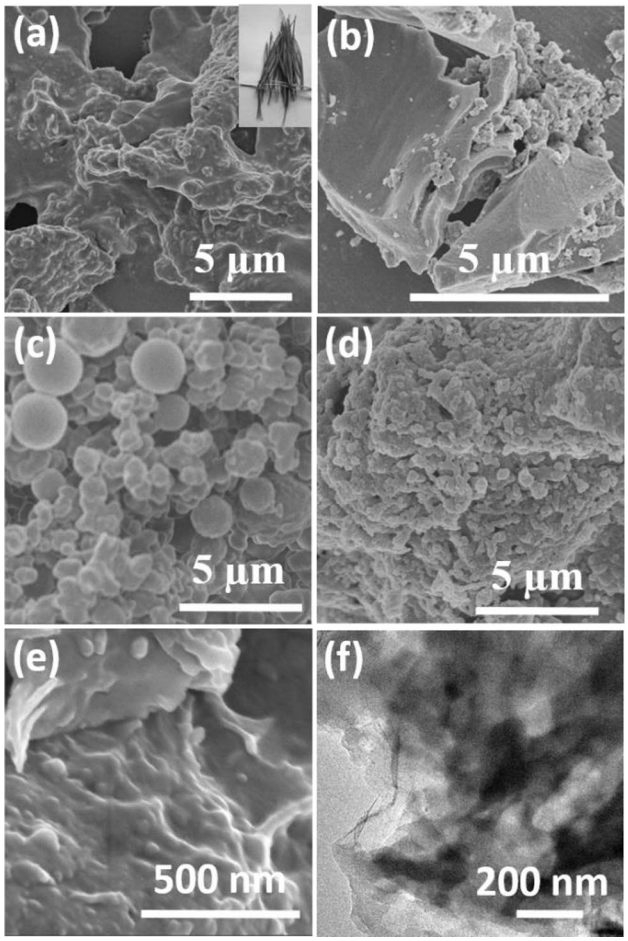

Fig. 1 **a** SEM image of pristine pine needle, the inset is the optical image of pristine pine needle; **b** SEM image of DPC; **c** SEM image of hydrothermal product; **d** SEM image of HTPC; **e**, **f** SEM and TEM images of HTPC/rGO composite

on the chars, further removing of oxygen and hydrogen is produced, and the chars become small. To reduce the surface energy, some nanoparticles prone to agglomerate, thus pine needle derived micro/nanostructure is obtained (named as HTPC) (Fig. 1d). As shown in Fig. 1d, some nanoparticles with the size about 40 nm agglomerated into bulk and the pores among the nanoparticles can be observed clearly. It is the common problem that hard carbons (DPC and HTPC) have low electronic conductivity, which would be the limiting step and have negative effect on the performance.

Compared with DPC, HTPC could offer higher capacity due to nanoparticles that can provide short transport distance for Na-ion and the much pores of HTPC endow more Na-ion diffuse into the electrode fast. To further improve the electronic conductivity of HTPC, rGO coating was employed, because of the superior electronic conductivity and well mechanical flexibility of rGO. GO was synthesized by the modified Hummers methods, as reported elsewhere [28]. The HTPC/rGO composite was prepared by a one-step high temperature annealing of HTPC and GO mixture process. The high temperature annealing not only reduces GO into rGO, but also coats rGO on the surface of HTPC simultaneously. The resulted product is showed in Fig. 1e; rGO is closely coated on HTPC, and some pores of HTPC are still exposed. Figure 1f shows the transmission electron microscopy (TEM) image of HTPC/rGO, which provides further evidence that rGO is thoroughly covered on the micro/nanostructure derived carbon of HTPC.

Figure 2 shows the structure characteristic of DPC, HTPC and HTPC/rGO composite. As indicated by X-ray diffraction (XRD) patterns (Fig. 2a), all three products are amorphous with two broad peaks at $2\theta = 23°$ and 44°, which can be ascribed to the (002) and (100) facets, respectively. $D_{(002)}$ was calculated to be 0.39 nm and the large interlayer spacing is favorable for reversible storage of large diameter of sodium ions (1.02 Å). The corresponding Raman spectra are shown in Fig. 2b; two peaks are observed at 1350 cm^{-1} (D-band) and 1590 cm^{-1} (G-band) for the three samples, respectively. The intensity ratios of the D-band to the G-band (ID/IG) for the three samples approach 1, which are similar to most other amorphous carbon materials [31-33]. The porous structure is analyzed by N_2 sorption test. The BET surface areas for DPC and HTPC are 1.2 and 141 $m^2\ g^{-1}$, respectively. Combined with the results of XRD and Raman, the derived ones are hard carbon, and hard carbon can accommodate sodium ions in enlarged graphene-like layers and nanopores [34–36].

All derived carbons were tested as the anode of SIBs in the coin cells (2032), the metallic sodium was used as both counter and reference electrodes. As shown in Fig. 3a, DPC has the first-cycle Coulombic efficiency of 62%, which is higher than that of HTPC (60%), but the discharge capacity is only 67% of HTPC at the 50th cycle. As the smaller surface area of DPC (1.2 $m^2\ g^{-1}$) than that of HTPC (141 $m^2\ g^{-1}$), a limit contact bewteen eletrode and electrolyte results in the high first-cycle Coulombic efficiency of DPC. The long diffusion distance form the surface to the bulk of electrode for DPC is disadvantage for sodium ion and electron transport. So, the capacity of DPC is smaller than that of HTPC. The decreased capacity from 1st cycle to the subsequent cycles of HTPC is resulted from the formation of solid electrolyte interface (SEI) film and electrolyte decomposition, which can be evidenced by the area difference between the first cycle and subsequent cycle of the cyclic voltammograms (CV) curves. Figure 3b shows the detailed consecutive first three CV curves of HTPC electrode between 0.01 and 3.0 V at a scan rate of 0.1 mV s^{-1}. The redox peaks (0.01–0.1 V and 0.2–0.5 V) appeared in all cycles corresponding to sodium-ion insert reversiblely into graphite layers of the disordered carbon, which reflected on the discharge curve is the slop region [37], while the plateau

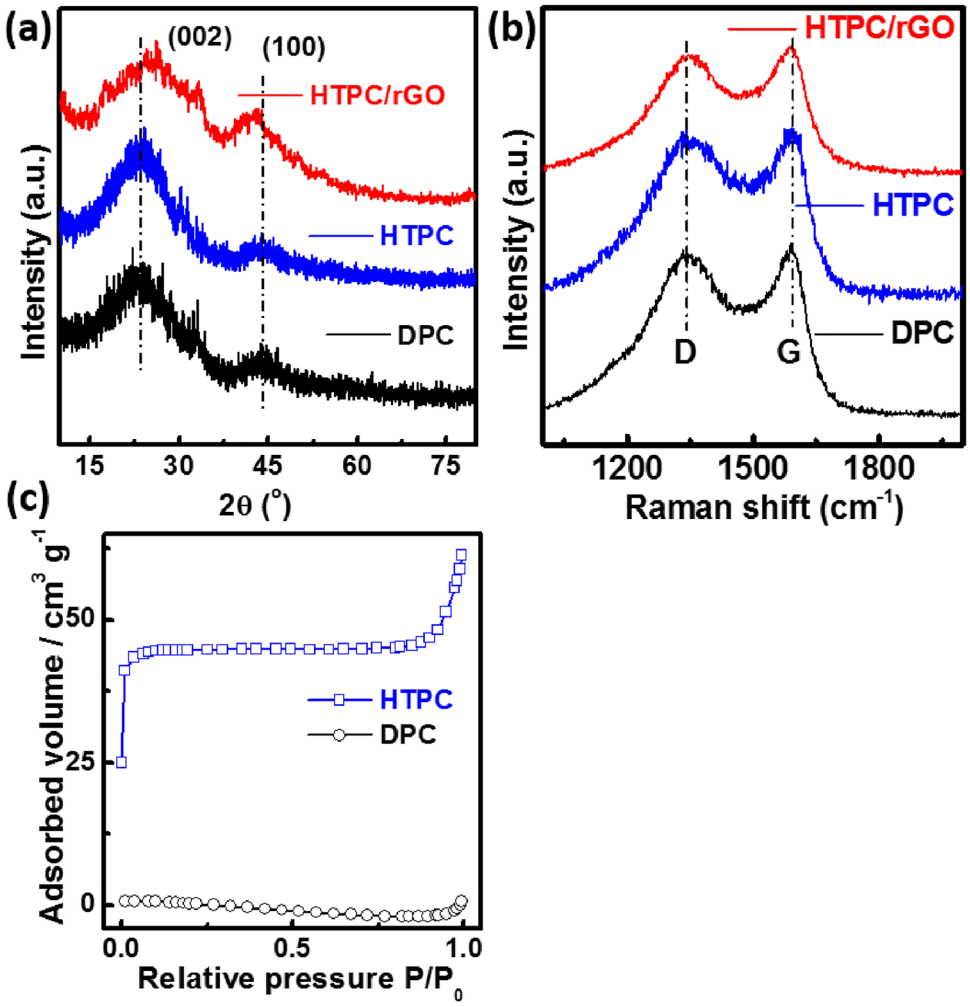

Fig. 2 **a** XRD patterns and **b** Raman spectra of DPC, HTPC and HTPC/rGO composite. **c** N_2 sorption isotherms of DPC and HTPC

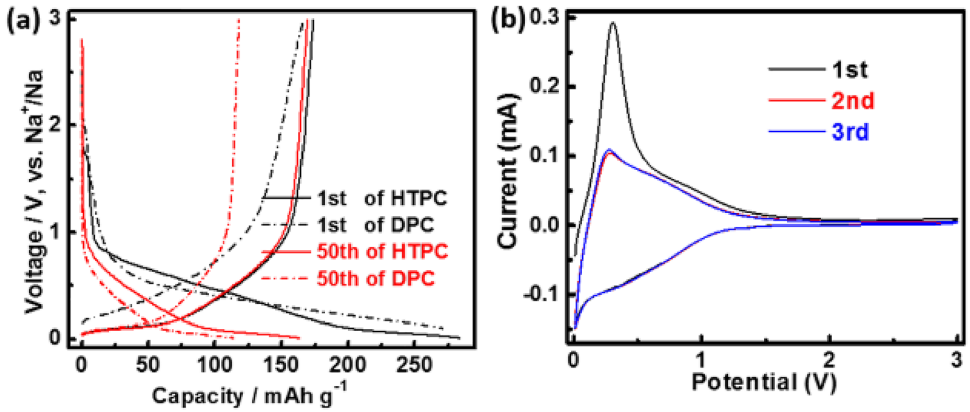

Fig. 3 **a** Galvanostatic charge/discharge curves of HTPC and DPC electrodes at 20 mA g^{-1}, **b** CV profiles of HTPC electrode

region of the discharge curve is assigned to the mechanism of sodium reversible insertion into nanopores.

As the high capacity and moderate first-cycle Coulombic efficiency of HTPC, we choose it to coat rGO to futher improve the electrochemical performance. Figure 4a shows the galvanostatic charge/discharge curves of HTPC/rGO, and the discharge capacity of the 1st, 2nd and 100th cycle is 525, 283 and 281 mAh g^{-1} at the current density of 20 mA g^{-1}. The discharge capacity of HTPC is only 284, 177 and 167 mAh g^{-1} of the corresponding cycles at 20 mA g^{-1}. The improved capacity is mostly resulted form the enhanced electrical conductivity by modification rGO, due to rGO only has the capacity of 31 mAh g^{-1} about as reported [13] and its content was little. It also increases the rate

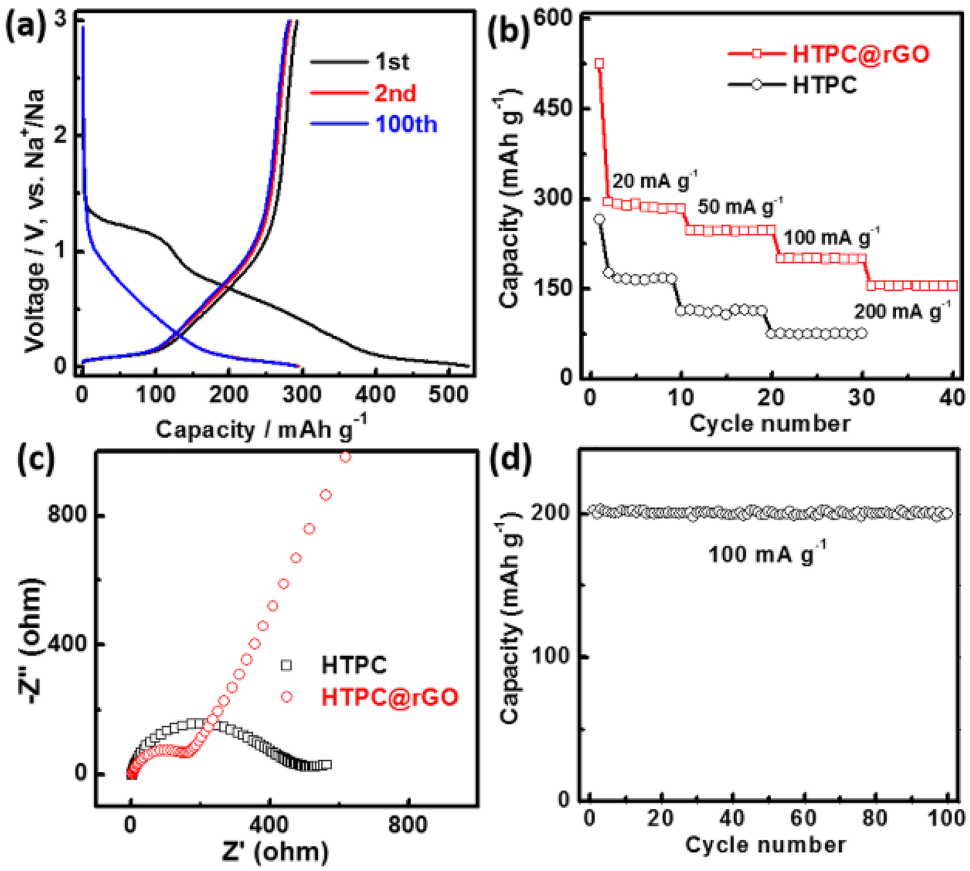

Fig. 4 **a** Galvanostatic charge/discharge curves of HTPC/rGO electrode at 20 mA g^{-1}, **b** rate profiles of HTPC/rGO and HTPC electrodes, **c** Nyquist plot of HTPC/rGO and HTPC electrodes and **d** cycling performance for HTPC/rGO electrode at 100 mA g^{-1}

performance, as shown by Fig. 4b. HTPC/rGO dilivers the discharge capacity of 281, 248, 200 and 156 mAh g^{-1} at the current density of 20, 50 100 and 200 mA g^{-1}, respectively. Figure 4c demonstrates the electrochemical impedance spectroscopy at a potential of 5 mV within a frequency range of 10 kHz to 0.01 Hz for HTPC and HTPC/rGO; the smaller semicircle of HTPC/rGO than that of HTPC reveals the decreased charge-transfer resistance and increased electrical conductivity, which are ascribed to outstanding conductivity of rGO. HTPC/rGO also exhibits well cycle stability (Fig. 4d), and at 100 mA g^{-1}, the capacity is retained of 99% after 100 cycles. So, after coating rGO, the electrochemistry performance had a much enhance. rGO could be effective for other hard carbon.

4 Conclusions

In this work, pine needle derived bulk and micro/nanostructure hard carbons were obatined by direct pyrolysis and hydrothermal followed pyrolyzation treatments, respectively. Because some Na ions could be stored in the nanopores, the small surface area of the bulk amorphous carbon resulted in low capacity. The derived micro/nanostructure hard carbon displays moderate capacity. In order to improve the electrochemical performance, rGO coating is employed for the micro/nanostructure carbon by a one-step high temperature annealing process. Due to the enhanced electrical conductivity, HTPC/rGO composite displays the capacity of 281 mAh g^{-1} at 20 mA g^{-1}, which is improved by 68%. Well rate performance and long-cycle stability are also obtained. Considering the improved performance and bio-renewable advantage, the micro/nanostructure hard carbon derived from pine needle coated with rGO would be a suitable anode material for SIBs.

References

1. M. Li, J. Lu, Z. Chen, K. Amine, Adv. Mater. **30**, 1800561 (2018)
2. Y. Liu, Q. Liu, A. Zhang, J. Cai, X. Cao, Z. Li, P.D. Asimow, C. Zhou, ACS Nano **12**, 8323 (2018)
3. P. Zheng, J. Su, Y. Wang, W. Zhou, J. Song, Q. Su, N. Reeves-McLaren, S. Guo, ChemSusChem **13**, 1793 (2020)
4. P. Wu, A. Zhang, L. Peng, F. Zhao, Y. Tang, Y. Zhou, G. Yu, ACS Nano **12**, 759 (2018)
5. M.D. Slater, D. Kim, E. Lee, C.S. Johnson, Adv. Funct. Mater. **23**, 947 (2012)
6. L.P. Wang, L. Yu, X. Wang, M. Srinivasan, Z.J. Xu, J. Mater. Chem. A **3**, 9353 (2015)
7. D. Kundu, E. Talaie, V. Duffort, L.F. Nazar, Angew. Chem. Int. Ed. **54**, 3431 (2015)

8. K. Kubota, N. Yabuuchi, H. Yoshida, M. Dahbi, S. Komaba, MRS Bull. **39**, 416 (2014)
9. M. Fan, Z. Lin, P. Zhang, X. Ma, K. Wu, M. Liu, X. Xiong, Adv. Energy Mater. **11**, 2003037 (2021)
10. R. Sagar, A.S. Gandhi, Appl. Phys. A **127**, 84 (2021)
11. P. Ge, M. Fouletier, Solid State Ion. **28**, 1172 (1988)
12. W. Luo, C. Bommier, Z. Jian, X. Li, R. Carter, S. Vail, Y. Lu, J.-J. Lee, X. Ji, A.C.S. Appl, Mater. Interfaces **7**, 2626 (2015)
13. Y. Wen, K. He, Y. Zhu, F. Han, Y. Xu, I. Matsuda, Y. Ishii, J. Cumings, C. Wang, Nat. Commun. **5**, 4033 (2014)
14. A. Massaro, A.B. Muñoz-García, P. Maddalena, F. Bella, G. Meligrana, C. Gerbaldi, M. Pavone, First-principles study of Na insertion at TiO_2 anatase surfaces: new hints for Na-ion battery design. Nanoscale Adv. **2**, 2745 (2020)
15. Z. Hong, H. Maleki, T. Ludwig, Y. Zhen, M. Wilhelm, D. Lee, K.-H. Kim, S. Mathur, New insights into carbon-based and MXene anodes for Na and K-ion storage: a review. J. Energy Chem. **62**, 660 (2021)
16. J. Wu, J. Liu, J. Cui, S. Yao, M. Ihsan-Ul-Haq, N. Mubarak, E. Quattrocchi, F. Ciucci, J.-K. Kim, Dual-phase MoS_2 as a high-performance sodium-ion battery anode. J. Mater. Chem. A **8**, 2114 (2020)
17. F. Bella, F. Colò, J.R. Nair, C. Gerbaldi, Photopolymer electrolytes for sustainable, upscalable, safe, and ambient-temperature sodium-ion secondary batteries. ChemSusChem **8**, 3668 (2015)
18. G. Zhang, J. Shu, L. Xu, X. Cai, W. Zou, L. Du, S. Hu, L. Mai, Pancake-like MOF solid-state electrolytes with fast ion migration for high-performance sodium battery. Nano-Micro Lett. **13**, 105 (2021)
19. Y. Li, Y. Yang, Y. Lu, Q. Zhou, X. Qi, Q. Meng, X. Rong, L. Chen, Y.-S. Hu, Ultralow-concentration electrolyte for Na-ion batteries. ACS Energy Lett. **5**, 1156 (2020)
20. D.A. Stevens, J.R. Dahn, J. Electrochem. Soc. **147**, 1271 (2000)
21. C. Bommier, T.W. Surta, M. Dolgos, X. Ji, Nano Lett. **15**, 5888 (2015)
22. T. Chen, L. Pan, T. Lu, C. Fu, D.H.C. Chua, Z. Sun, J. Mater. Chem. A **2**, 1263 (2014)
23. Y.M. Li, S.Y. Xu, X.Y. Wu, J.Z. Yu, Y.S. Wang, Y.S. Hu, H. Li, L.Q. Chen, X.J. Huang, J. Mater. Chem. A **3**, 71 (2015)
24. W. Chen, D. Deng, ACS Sustain. Chem. Eng. **3**, 63 (2015)
25. K.-L. Hong, L. Qie, R. Zeng, Z.-Q. Yi, W. Zhang, D. Wang, W. Yin, C. Wu, Q.-J. Fan, W.-X. Zhang, Y.-H. Huang, J. Mater. Chem. A **2**, 12733 (2014)
26. P. Zheng, T. Liu, S. Guo, Sci. Rep. **6**, 35620 (2016)
27. W. Luo, Z. Jian, Z. Xing, W. Wang, C. Bommier, M.M. Lerner, X. Ji, ACS Cent. Sci. **1**, 516 (2015)
28. J. Zhang, H. Yang, G. Shen, P. Cheng, J. Zhang, S. Guo, Chem. Commun. **46**, 1112 (2010)
29. V.K. Thakur, M.K. Thakur, P. Raghavan, M.R. Kessler, ACS Sustain. Chem. Eng. **2**, 1072 (2014)
30. P. Zheng, T. Liu, Y. Liu, L. Zhang, J. Huang, S. Guo, J. Zhang, RSC Adv. **5**, 40737 (2015)
31. W. Luo, J. Schardt, C. Bommier, B. Wang, J. Razink, J. Simonsen, X. Ji, J. Mater. Chem. A **1**, 10662 (2013)
32. R. Zou, Q. Liu, G. He, M.F. Yuen, K. Xu, J. Hu, I.P. Parkin, C.-S. Lee, W. Zhang, Adv. Energy Mater. **7**, 1601363 (2017)
33. F.J. Martin-Martinez, K. Jin, D. López Barreiro, M.J. Buehler, ACS Nano **12**, 7425 (2018)
34. H. Kim, J. Hong, Y.-U. Park, J. Kim, I. Hwang, K. Kang, Adv. Funct. Mater. **25**, 534 (2015)
35. T. Chen, Y. Liu, L. Pan, T. Lu, Y. Yao, Z. Sun, D.H.C. Chua, Q. Chen, J. Mater. Chem. A **2**, 4117 (2014)
36. S. Li, J. Qiu, C. Lai, M. Ling, H. Zhao, S. Zhang, Nano Energy **12**, 224 (2015)
37. Y. Shao, J. Xiao, W. Wang, M. Engelhard, X. Chen, Z. Nie, M. Gu, L.V. Saraf, G. Exarhos, J.-G. Zhang, J. Liu, Nano Lett. **13**, 3909 (2013)